AD-A125 217 IGNITION OF FLAMELETS BEHIND INCIDENT SHOCK WAVES AND THE TRANSITION TO DETONATION(U) NAVAL RESEARCH LAB WASHINGTON DC K KAILASANATH ET AL. 07 MAR 83 1/1

UNCLASSIFIED NRL-MR-5030 F/G 21/2 NL

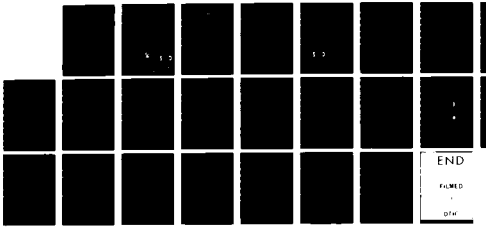

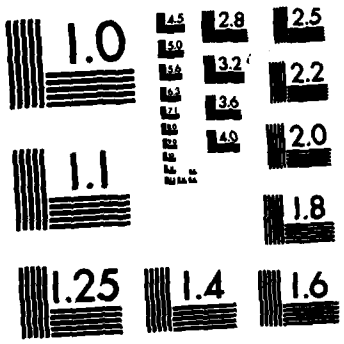

NRL Memorandum Report 5030

(2)

Ignition of Flamelets Behind Incident Shock Waves and the Transition to Detonation

K. KAILASANATH* AND E. S. ORAN

Laboratory for Computational Physics

**Science Applications Inc.*
McLean, VA 22102

March 7, 1983

This work was supported by the Office of Naval Research.

NAVAL RESEARCH LABORATORY
Washington, D.C.

SECURITY CLASSIFICATION OF THIS PAGE (When Data Entered)

REPORT DOCUMENTATION PAGE		READ INSTRUCTIONS BEFORE COMPLETING FORM
1. REPORT NUMBER NRL Memorandum Report 5030	2. GOVT ACCESSION NO. A125217	3. RECIPIENT'S CATALOG NUMBER
4. TITLE (and Subtitle) IGNITION OF FLAMELETS BEHIND INCIDENT SHOCK WAVES AND THE TRANSITION TO DETONATION		5. TYPE OF REPORT & PERIOD COVERED Interim report on a continuing NRL problem. 6. PERFORMING ORG. REPORT NUMBER
7. AUTHOR(s) K. Kailasanath* and E.S. Oran		8. CONTRACT OR GRANT NUMBER(s)
9. PERFORMING ORGANIZATION NAME AND ADDRESS Naval Research Laboratory Washington, DC 20375		10. PROGRAM ELEMENT, PROJECT, TASK AREA & WORK UNIT NUMBERS 61153N; RR0130646; 44-1519-0-3
11. CONTROLLING OFFICE NAME AND ADDRESS		12. REPORT DATE March 7, 1983 13. NUMBER OF PAGES 32
14. MONITORING AGENCY NAME & ADDRESS(if different from Controlling Office)		15. SECURITY CLASS. (of this report) UNCLASSIFIED 15a. DECLASSIFICATION/DOWNGRADING SCHEDULE

16. DISTRIBUTION STATEMENT (of this Report)

Approved for public release; distribution unlimited.

17. DISTRIBUTION STATEMENT (of the abstract entered in Block 20, if different from Report)

18. SUPPLEMENTARY NOTES

*Present address: Science Applications Inc., McLean, VA 22102

This work was supported by the Office of Naval Research.

19. KEY WORDS (Continue on reverse side if necessary and identify by block number)

Shock waves	Numerical simulation
Ignition	Flux-corrected transport
Detonation	Chemical kinetics

20. ABSTRACT (Continue on reverse side if necessary and identify by block number)

Time-dependent numerical simulations are used to elucidate some of the details of weak ignition behind incident shocks and the subsequent transition to detonation. It is shown that a small amount of energy released in the shocked region can be the origin of pressure waves which accelerate the shock front. The simulations presented here show how this leads to the formation of reactive centers. The formation of a hot spot due to energy

(Continues)

DD FORM 1 JAN 73 1473 EDITION OF 1 NOV 65 IS OBSOLETE
S/N 0102-014-6601

SECURITY CLASSIFICATION OF THIS PAGE (When Data Entered)

20. ABSTRACT (Continued)

release at one of the reactive centers and the subsequent development of a pair of flamelets from the hot spot are studied using the numerical simulations. The results of the simulations are also compared to experimental observations.

CONTENTS

IGNITION OF FLAMELETS BEHIND INCIDENT SHOCK WAVES AND THE TRANSITION TO DETONATION

I. INTRODUCTION

Shock-induced ignition in gaseous hydrogen-air mixtures may occur in one of two distinct modes, depending on the thermodynamic state in the shocked material. At lower temperatures the ignition is weak, or mild, with the gradual development of the gas dynamic explosion. At higher temperatures it is strong, or sharp, with an abrupt appearance of a secondary shock induced by the explosive reaction. Furthermore at low temperatures the formation of distinct flame kernels appears to be an essential precursor of ignition. Meyer and Oppenheim (1971a) point out that the intrinsically turbulent flow field behind a reflected shock in a shock tube results in a nonuniform temperature distribution which creates distinct reaction centers and leads to weak ignition. Although the nonuniformity of temperature caused by turbulence is one mechanism which gives rise to reaction centers, the nonsteadiness in the velocity of the causal shock can also produce them. This latter effect has been convincingly demonstrated by Strehlow et al. (1967) in their studies of shock propagation in a slowly converging channel. It has also been shown that when an incident shock in a uniform shock tube begins to accelerate, hot spots occur before the transition to detonation (Bazhenova and Soloukhin, 1959; Edwards et al., 1981).

In this paper the reactive flow behind an incident shock wave in a hydrogen-air mixture is simulated using a one-dimensional, time-dependent numerical model which combines a description of the fluid dynamics and detailed chemical kinetics. In the simulations, the pressure ratio across the diaphragm and the driven gas mixture are chosen so that the thermodynamic

Manuscript approved December 23, 1982.

state behind the incident shock is in the weak ignition regime (Oran and Boris, 1981b). It is shown that a small amount of energy released in the shocked gas (which might occur due to density, temperature or stoichiometric fluctuations) can be the origin of pressure waves which accelerate the shock front. Once the shock is accelerated, the temperature of the gases now passing through the shock is higher than the raised temperature created by the original shock. In the weak ignition regime, such an increased temperature can result in a significant reduction in the induction time (Meyer and Oppenheim. 1971b; Oran and Boris, 1981b). The simulations presented here show how this leads to the formation of reactive centers in the newly shocked material where reaction progresses at a more rapid rate than in the previously shocked material. The formation of a hot spot due to energy release at one of the reactive centers and the subsequent development of a pair of flamelets or reaction waves from the hot spot are studied using the numerical simulations. The results of the simulations have also been compared to experimental observations (Bazhenova and Soloukhin, 1959; Urtiew and Oppenheim, 1966, 1967; Strehlow et al., 1967; Edwards et al., 1981).

II. THE NUMERICAL MODEL

The one-dimensional reactive shock model (Oran et al., 1979; Oran and Boris, 1981a) used to perform the calculations described below solves the time-dependent conservation equations (Williams, 1965; Oran and Boris, 1981a) for mass, momentum and energy coupled to the equations describing the chemical kinetics. The model uses an explicit, Eulerian finite difference formulation with a sliding rezone capability to provide resolution around moving gradients. The solutions of the equations describing the fluid

dynamics and the chemistry of the problem are coupled using time-step splitting techniques (Oran and Boris, 1981a).

The convective transport terms in the conservation equations are solved using one variant of the Flux-Corrected Transport (FCT) method (Boris and Book, 1976; Boris, 1976). This is a conservative, monotonic algorithm with fourth-order phase accuracy and does not require artificial viscosity to stabilize shocks. The Flux Correction procedure itself ensures that the shocks are one or two zones wide and have maximal resolution. The ordinary differential equations describing the chemical kinetics are solved using VSAIM, a vectorized version of the selected asymptotic integration method employed in CHEMEQ (Young and Boris, 1977; Young, 1980). This algorithm identifies the stiff equations for treatment with a stiffly stable method. The remaining equations are solved with a standard classical method. The algorithm has been specially optimized for use in conjunction with fluid dynamic models.

The chemical kinetics rate scheme used is given in Table I. It consists of about fifty rates relating the species H_2, O_2, H, O, OH, HO_2, H_2O and H_2O_2 and has been extensively tested against experimental data (Oran et al., 1981, Burks and Oran, 1980). Burks and Oran (1980) showed that the results computed with the scheme compared very well with experimentally observed induction times, second explosion limits and the temporal behavior of reactive species. Oran et al. (1981) have shown that the scheme gives good results when coupled with a fluid dynamic model in the simulation of the conditions behind a reflected shock. Heats of formation and enthalpies have been taken from the JANAF tables (1971).

For the calculations performed in this paper, the timescales under consideration are short and therefore the diffusive transport processes, thermal conduction and molecular diffusion, have negligible effect. The effects of these processes have not been considered although they are part of the general numerical model. Although the geometry may be either cartesian, cylindrical, spherical or some generalized co-ordinate, the simulations presented below are in cartesian geometry.

The detailed simulations discussed in this paper require that we model relatively long systems (on the order of meters) while we simultaneously maintain high accuracy around steep gradients such as the shock front and the contact surface. The rather sophisticated adaptive gridding method developed for this purpose is shown schematically in Figure 1. There are two finely gridded regions: One surrounding the shock wave and the other surrounding the contact surface. The fine-zoned region around the contact surface moves with the contact surface at the fluid velocity, and so this part of the calculations is essentially Lagrangian. The region around the shock front moves with the front. Each of these finely gridded regions may have a different minimum computational cell size. The computational cells in the regions ahead of the shock wave and behind the contact surface change exponentially in size from the smallest near the shock wave or the contact surface to the largest at the walls. Care is taken that the transition in the cell sizes is smooth. For the results presented in this paper a total of 200 computational cells are used to describe the shock tube and the cell sizes varied from 0.1 cm around the shock to over 50 cm near the shock tube end-walls.

III. WEAK IGNITION BEHIND AN INCIDENT SHOCK

The numerical model described in the preceding section was used to study weak ignition behind planar incident shock waves. The system parameters, the initial conditions and the temperature and pressure behind the incident shock have all been summarized in Table II. The chemical induction time, for the conditions described by the incident shock, is about 2000 μs. However, since the thermodynamic state behind the shock is in the weak ignition regime, ignition may occur much earlier than 2000 μs due to temperature, pressure, or density fluctuations.

Figure 2 is a position-time diagram of the events occurring in the shock tube simulation. The trajectory of the shock front is labelled S and that of the contact surface is labelled CS. Except for small variations (which are examined in detail below) the shock travels at a nearly constant velocity, 1.4×10^5 cm/s, until the reaction wave formed between the contact surface and the shock front reaches it. At this time the velocity rises quickly to 3.24×10^5 cm/s. It then gradually decreases towards the Chapman-Jouguet detonation velocity. Five different regimes have also been identified on the diagram. They are (a) pre-ignition regime, (b) quasi-steady shock-reaction complex, (c) formation of reactive centers, (d) hot spot formation leading to an overdriven detonation and (e) detonation relaxation. Similar regions have been identified by Edwards et al. (1981) in their shock tube experiments. These regions are examined in detail below.

As the shock travels at a nearly constant velocity into the hydrogen-air mixture, the temperature and pressure of the mixture are raised to a near-constant value. Reactions in the shock heated gas first occur near the

contact surface since the temperature has been high for the longest time here, as has been observed by Urtiew and Oppenheim (1967). In Figure 3, the spatial variation of the temperature and the OH mole fraction between the shock and the contact surface are shown at 135 μs after the bursting of the diaphragm. The OH mole fraction attains a maximum value near the contact surface and decreases across the system towards the shock front. This is because the gas mixture at different locations has been at the higher temperature for different durations.

Formation of Reactive Centers and Hot Spots

Small pressure disturbances occur due to the energy released in the reactions near the contact surface. These pressure disturbances travel forward at a velocity (in the laboratory frame of reference) of 1.8×10^5 cm/s, which is the sum of the sonic and particle velocities behind the shock. When they reach the shock they accelerate the shock slightly resulting in a temperature increase behind the shock. This can be observed in Figure 4 where the spatial distribution of the temperature between the shock and the contact surface is shown at four different times. The nonuniform temperature distributions can be explained by the following sequence of events: pressure disturbances originating at different times near the contact surface reach the incident shock at different times and each successive pressure disturbance meets a shock of slightly different strength because the shock has already been accelerated slightly due to previous pressure disturbances. We know that in the weak ignition regime, the induction time is very sensitive to perturbations in temperature and pressure (Oran and Boris, 1981b). This sensitivity, in fact, is what produces the two peaks in OH mole

fraction distribution (Figure 5A) at 348 μs after the bursting of the diaphragm. The first peak is due to the development of reactions near the contact surface and occurs in the same reactive center (see Figure 2) which was observed earlier. Now a second reactive center has formed closer to the shock front due to the higher temperature created by the acceleration of the shock. Again we observe that the reactive center occurs in that part of the shock heated gas which was at the elevated temperature for the longest period of time. Ahead of the second reactive center the rapid decrease in the radical mole fraction is halted by a further increase in the temperature behind the shock and a third reactive center is forming. By 445 μs (Figure 5B), a third reactive center has developed and the radical mole fraction is rising most rapidly at this center. The temperature around this reactive center is significantly (about 40° K) greater than that behind the initial incident shock wave. In the weak ignition regime, such changes in temperature result in a substantial reduction in the induction time. Therefore reaction progresses at this reactive center at a much more rapid rate than at any other location in the system. This results in a "hot spot" in the system. The development of this hot spot can be seen in Figure 6 where the temperature distribution between the contact surface and the shock front has been shown for four different times. The temperature increases by more than 200° in 30 μs.

Transition to Detonation

The events occurring after the hot spot formation can be seen in Figure 7 where a segment of the position-time diagram (Figure 2) is presented in greater detail. The hot spot (marked "A" in the figure) travels with the

fluid and continuously releases energy into it. This results in "flamelets" or "reaction waves" ("B") which travel with respect to the fluid. One reaction wave moves forward with the fluid while another moves against the fluid towards the driver section. These reaction waves initially move subsonically with respect to the fluid but are soon accelerated into steep detonation type waves which move supersonically with respect to the fluid. When the forward moving reaction wave reaches the shock front, the shock velocity abruptly increases to a high value. The shock-reaction complex then moves as a strong overdriven detonation wave which decelerates towards the Chapman-Jouguet detonation velocity.

The temperature, pressure and velocity distributions across the system at a particular time after the hot spot has formed are shown in Figure 8a. By this time the energy release has resulted in a noticeable pressure rise. This occurs because the energy release is occurring at nearly constant volume conditions. The energy release at the hot spot causes a series of minute pressure pulses to propagate both forward and backward, each a little stronger than the previous one. A series of pressure pulses are produced since the energy release occurs over a period of time and is determined at each time from the detailed chemical kinetic interactions among the various species. These pressure pulses coalesce to form steepening pressure waves propagating into the shocked mixture as seen in Figure 8b. The time history of these reaction waves has been shown in a series of figures (Fig. 8b - Fig. 10b) which cover the time period between 609 μs and 688 μs.

Let us first look at the development of the reaction wave which moves forward into the shock-heated gas mixture. The velocity of the forward

moving wave, the fluid velocities on both sides of the wave and the speed of sound in the gas mixtures on both sides of the wave are given in Table III for a series of times. At 609 μs, the forward moving reaction wave is supersonic. The velocity of the fluid with respect to the wave decreases across the wave but is supersonic on either side. Furthermore the pressure rise across the wave is just over a factor of two, which is moderate. Thus the reaction wave behaves like a weak detonation wave at this time. Later, as seen in Figure 9a, the pressure rise across the wave has increased and the wave is also travelling faster. The velocity of the fluid with respect to the wave is still supersonic on both sides of the wave. The pressure rise across the wave continues to increase and at the time corresponding to Figure 9b, the fluid velocity behind the wave is nearly sonic. The weak detonation seems to be transitioning into a strong detonation. It does so later (Figure 9c) when the fluid velocity changes from supersonic to subsonic across the reaction wave. The pressure rise across the wave is also larger now. The observed acceleration of the forward moving wave into a strong detonation is due to the nonlinear interaction between chemical kinetics and fluid dynamics. When the forward moving wave moves into the previously shocked material there is a large pressure and temperature rise across it since it is a strong compressive wave. This increase in the pressure and the temperature reduces the induction time of the material which crossed the wave. Energy release in this newly re-compressed material accelerates the forward moving wave further, and this cycle is repeated until the forward moving wave reaches the incident shock wave (Figure 10a). By this time the pressure spike behind the reaction wave has risen to 6.6×10^6 dynes/cm^2. Because the

reaction wave is moving towards the incident shock at a speed greater than the local speed of sound in the shock-heated gas, there is no advance warning of the over-pressure region until the main spike physically arrives at the shock front. When the reaction wave does coalesce with the shock, there is a very rapid increase in the shock speed (Figure 7) and the shock-reaction wave complex moves as an overdriven strong detonation wave. Due to the high over-pressure that was associated with the reaction front, the detonation wave overshoots the Chapman-Jouguet value by a substantial amount. However, the overshoot cannot be sustained by the reaction and the overdriven detonation gradually relaxes towards a Chapman-Jouguet wave. By 688 μs (Figure 10b) the pressure spike behind the detonation wave has decreased to 4.8×10^6 dynes/cm^2 and the wave is moving faster than the C-J velocity by only 36%. In Figure 10b we also observe a small amplitude pressure wave moving into the detonation products. This pressure wave was formed when the reaction wave interacted with the shock front.

Let us now look at the reaction wave which moves backward towards the driver section. From Figure 7 and Table IV we see that this wave moves at nearly the sonic speed. The fluid velocity with respect to the wave is supersonic on either side of the wave. The pressure rise and the acceleration of the wave are slower since the wave is moving against the fluid. The pressure increase behind the wave is broader (Figure 9c) and smaller than that of the forward moving wave. It continues to propagate like a weak detonation wave until it interacts with the contact surface (Figure 10a). This interaction produces a pressure pulse which travels into the helium driver gas. In Figure 10b we see that this pressure pulse has produced a slight temperature increase in the helium.

IV. DISCUSSION AND CONCLUSIONS

In this paper the reactive flow behind an incident shock wave has been studied using a time-dependent numerical model which includes both detailed chemical kinetics and one-dimensional fluid dynamics. The numerical simulations show that the incident shock initially travels at a steady speed leaving behind it material in what has been called a "quasi-steady reaction complex". From their extensive experimental studies on detonation, Lee et al. (1976, 1977) have concluded that such regimes are universal predetonation phenomena. This regime has also been observed in the incident shock tube experiments of Edwards et al. (1981).

The calculations have also shown the acceleration of the shock due to pressure waves created by energy release in the shock heated gas mixture, a phenomenon also observed by Edwards et al. (1981). Shock acceleration raises the temperature of the gases passing through the shock and in the weak ignition regime, this results in a significant reduction of the induction time (Meyer and Oppenheim, 1971b; Oran and Boris, 1981b). This leads to the formation of reactive centers where reaction progresses at a more rapid rate than in the previously shocked material. The development of a hot spot due to energy release at one of the reactive centers has been shown in Figure 6. The presence of such hot spots has been observed earlier in shock tube experiments (Strehlow et al., 1967, Edwards et al., 1981).

Energy release at a hot spot causes a pair of flamelets or reaction waves, one propagating ahead into the shock heated gas mixture and the other propagating back towards the contact surface. These flamelets initially propagate at a subsonic speed with respect to the fluid. Such flamelets have

been observed by Bazhenova and Soloukhin (1959) in their incident shock tube experiments. Energy release behind these flamelets causes pressure waves which accelerate the flamelets into detonation type waves. The reaction wave moving backward against the fluid accelerates slowly and travels at nearly the sonic speed till it reaches the contact surface. However the forward moving reaction wave transitions into a strong detonation wave even before it reaches the incident shock wave. This agrees with the observation made by Bazhenova and Soloukhin (1959) that the merging of the flame front with the incident shock wave is not a necessary condition for the detonation wave formation. The simulations also show a large pressure overshoot when the forward moving wave coalesces with the incident shock wave. This has been observed earlier in the experiments of Urtiew and Oppenheim (1966).

The numerical simulations presented in this paper show that the one-dimensional reactive flow model with detailed chemical kinetics can be used to elucidate some of the details of weak ignition behind incident shocks and the subsequent transition to detonation. The predictions of the model are in qualitative agreement with experimental observations. However, the model does not include multi-dimensional phenomena such as turbulence and boundary layer growth which play an important part in any quantitative study of the transiton to detonation. Currently a two-dimensional reactive shock model exists but it uses a parameterized model for energy release (Oran et al., 1981b; Oran et al., 1982). The model is now being extended to include a detailed chemical kinetic scheme. Calculations with this new model would show the effects of transverse waves and boundary layers on the transition to detonation.

Table I. H_2-O_2 Elementary Reaction Mechanism

Reaction	$k_1 = AT^B \exp(-C/T)$[a] A[b]	B	C[b]	References[c]
$H + HO \rightleftarrows O + H_2$	1.40(-14)	1.00	3.50(+03)	[1]
	3.00(-14)	1.00	4.48(+03)	[1]
$H + HO_2 \rightleftarrows H_2 + O_2$	4.20(-11)	0.00	3.50(+02)	[1]
	9.10(-11)	0.00	2.91(+04)	[1]
$H + HO_2 \rightleftarrows HO + HO$	4.20(-10)	0.00	9.50(+02)	[1]
	2.00(-11)	0.00	2.02(+04)	[1]
$H + HO_2 \rightleftarrows O + H_2O$	8.30(-11)	0.00	5.00(+02)	[2]
	1.75(-12)	0.45	2.84(+04)	$k_r = k_f/K_c$
$H + H_2O_2 \rightleftarrows HO_2 + H_2$	2.80(-12)	0.00	1.90(+03)	[1]
	1.20(-12)	0.00	9.40(+03)	[1]
$H + H_2O_2 \rightleftarrows HO + H_2O$	5.28(-10)	0.00	4.50(+03)	[1]
	3.99(-10)	0.00	4.05(+04)	$k_r = k_f/K_c$
$HO + H_2 \rightleftarrows H + H_2O$	1.83(-15)	1.30	1.84(+03)	[3]
	1.79(-14)	1.20	9.61(+03)	[3]
$HO + HO \rightleftarrows H_2 + O_2$	1.09(-13)	0.26	1.47(+04)	$k_f = k_r K_c$
	2.82(-11)	0.00	2.42(+04)	[4]
$HO + HO \rightleftarrows O + H_2O$	1.00(-16)	1.30	0.00(+00)	[3]
	3.20(-15)	1.16	8.77(+03)	$k_r = k_f/K_c$
$HO + HO_2 \rightleftarrows H_2O + O_2$	8.30(-11)	0.00	5.03(+02)	[5]
	2.38(-10)	0.17	3.69(+04)	$k_r = k_f/K_c$
$HO + H_2O \rightleftarrows HO_2 + H_2$	1.70(-11)	0.00	9.10(+02)	[1]
	4.70(-11)	0.00	1.65(+04)	[1]
$HO + H_2 \rightleftarrows HO + H_2O$	1.20(-12)	0.00	9.41(+03)	[4]
	1.33(-14)	0.43	3.62(+04)	$k_r = k_f/K_c$
$HO_2 + HO_2 \rightleftarrows H_2O_2 + O_2$	3.00(-11)	0.00	5.00(+02)	[2]
	1.57(-09)	-0.38	2.20(+04)	$k_r = k_f/K_c$

Table I. (Continued) H_2-O_2 Elementary Reaction Mechanism

Reaction	$k_i = AT^B \exp(-C/T)$[a] A[b]	B	C[b]	References[c]
O+ HO ⇕ H + O_2	2.72(-12)	0.28	-8.10(+01)	$k_f = k_r K_c$
	3.70(-10)	0.00	8.45(+03)	[1]
O + HO_2 ⇕ HO + O_2	8.32(-11)	0.00	5.03(+02)	[5]
	2.20(-11)	0.18	2.82(+04)	$k_r = k_f/K_c$
O + H_2O_2 ⇕ H_2O + O_2	1.40(-12)	0.00	2.12(+03)	[2]
	5.70(-14)	0.52	4.48(+04)	$k_r = k_f/K_c$
O + H_2O_2 ⇕ HO + HO_2	1.40(-12)	0.00	2.13(+03)	[2]
	2.07(-15)	0.64	8.23(+03)	$k_r = k_f/K_c$
H + H + M ⇕ H_2 + M	1.80(-30)	-1.00	0.00(+00)	[1]
	3.70(-10)	0.00	4.83(-04)	[1]
H + HO + M ⇕ H_2O + M	6.20(-26)	-2.00	0.00(+00)	[1]
	5.80(-09)	0.00	5.29(+04)	[1]
H + O_2 + M ⇕ HO_2 + M	4.14(-33)	0.00	-5.00(+02)	[1]
	3.50(-09)	0.00	2.30(+04)	[1]
HO + HO + M ⇕ H_2O_2 + M	2.50(-33)	0.00	-2.55(+03)	[1]
	2.00(-07)	0.00	2.29(+04)	[1]
O + H + M ⇕ HO + M	8.28(-29)	-1.00	0.00(+00)	[6]
	2.33(-10)	0.21	5.10(+04)	$k_r = k_f/K_c$
O + HO + M ⇕ HO_2 + M	2.80(-31)	0.00	0.00(+00)	[6]
	1.10(-04)	-0.43	3.22(+04)	$k_r = k_f/K_c$
O + O + M ⇕ O_2 + M	5.20(-35)	0.00	-9.00(+02)	[1]
	3.00(-06)	-1.00	5.94(+04)	[1]

(a) Bimolecular reaction rate constants are given in units of $cm^3/(molecule\ sec)$. Termolecular reaction rate constants are given in units of $cm^6/(molecule^2\ sec)$.

(b) Exponentials to the base 10 are given in parenthesis; i.e., 1.00(-10) = 1.00×10^{-10}.

(c) The references are: (1) Baulch et al., 1972; (2) Hampson and Garvin, 1975; (3) Cohen and Westberg, 1979; (4) Olson and Gardiner, 1977; (5) Lloyd, 1974; (6) Bahn, 1968.

Table II. Parameters for the Weak Ignition Study.

Parameter	Driver Section	Driven Section
Length	30 cm	370 cm
Gas Mixture	He	$H_2:O_2:N_2/2:1:4$
Initial Temperature	298 K	298 K
Initial Pressure	9 atm	0.1 atm
Incident Shock Velocity		1.4×10^5 cm/s
Temperature behind Incident Shock		918 K
Pressure behind Incident Shock		1.39 atm
Chapman-Jouguet Detonation Velocity		1.9×10^5 cm/s

Table III. Time History of the Forward Moving Reaction Wave.

Time (μs)	Velocity of Wave (cm/s)	Fluid Velocity (cm/s)		Sound Velocity (cm/s)	
		Ahead	Behind	Ahead	Behind
609.03	2.70(+05)	1.09(+05)	1.30(+05)	7.15(+04)	1.10(+05)
618.63	2.72(+05)	1.08(+05)	1.50(+05)	7.15(+04)	1.12(+05)
626.03	2.75(+05)	1.08(+05)	1.60(+05)	7.10(+04)	1.15(+05)
631.83	2.80(+05)	1.08(+05)	1.85(+05)	7.08(+04)	1.14(+05)
663.83	3.20(+05)	1.07(+05)	2.10(+05)	7.20(+04)	1.18(+05)
688.13	2.60(+05)	0	2.10(+05)	4.04(+04)	1.28(+05)

Note: Exponentials to the base 10 are given in parenthesis, i.e., $2.70(+05) = 2.70\times10^5$

Table IV. Time History of the Backward Moving Reaction Wave.

Time (μs)	Velocity of Wave (cm/s)	Fluid Velocity (cm/s)		Sound Velocity (cm/s)	
		Ahead	Behind	Ahead	Behind
609.03	-7.2(+04)	1.08(+05)	8.3(+05)	7.2(+04)	1.06(+05)
618.63	-7.3(+04)	1.08(+05)	7.0(+04)	7.2(+04)	1.11(+05)
626.03	-7.5(+04)	1.09(+05)	6.0(+04)	7.2(+04)	1.13(+05)
631.83	-7.6(+04)	1.09(+05)	5.5(+04)	7.2(+04)	1.14(+05)

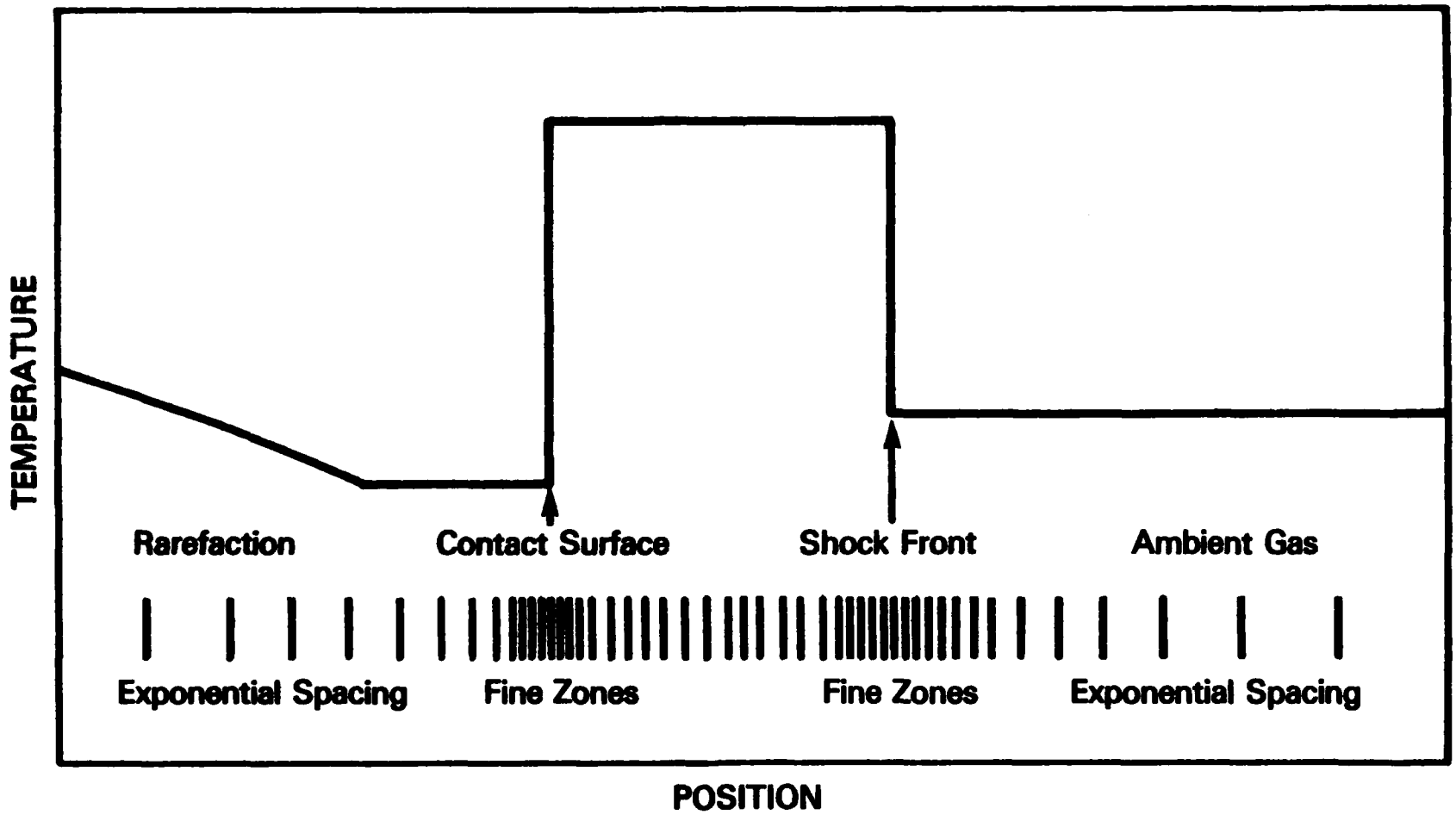

Figure 1. A schematic representation of the adaptive grid used for the numerical simulations.

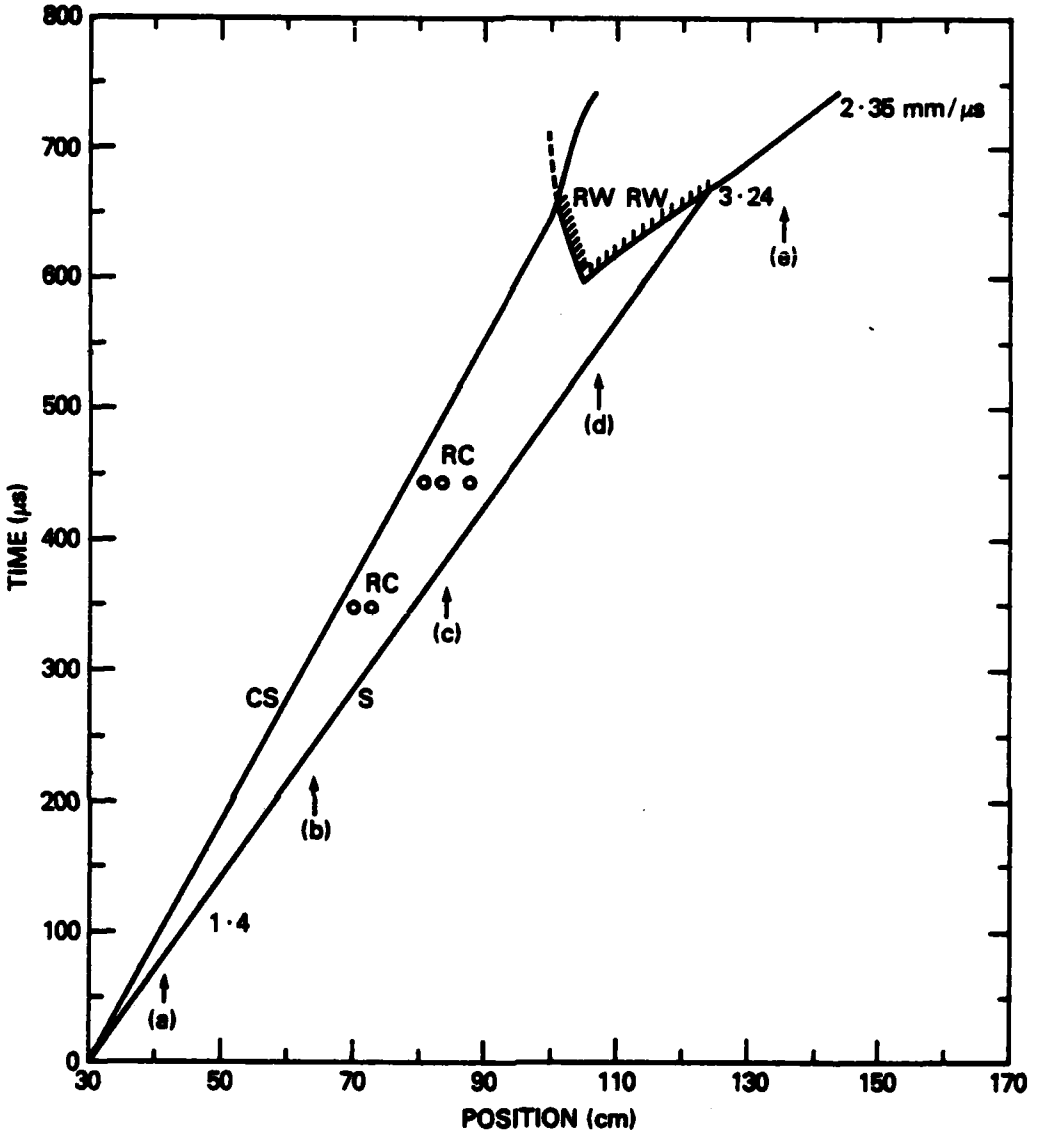

Figure 2. A position-time diagram of the main events occurring in the shock tube simulation: S, incident shock; CS, contact surface; RC, reactive centers, RW, reaction wave; (a) pre-ignition regime, (b) quasi-steady shock-reaction complex, (c) formation of reactive centers, (d) hot spot formation leading to overdriven detonation and (e) detonation relaxation.

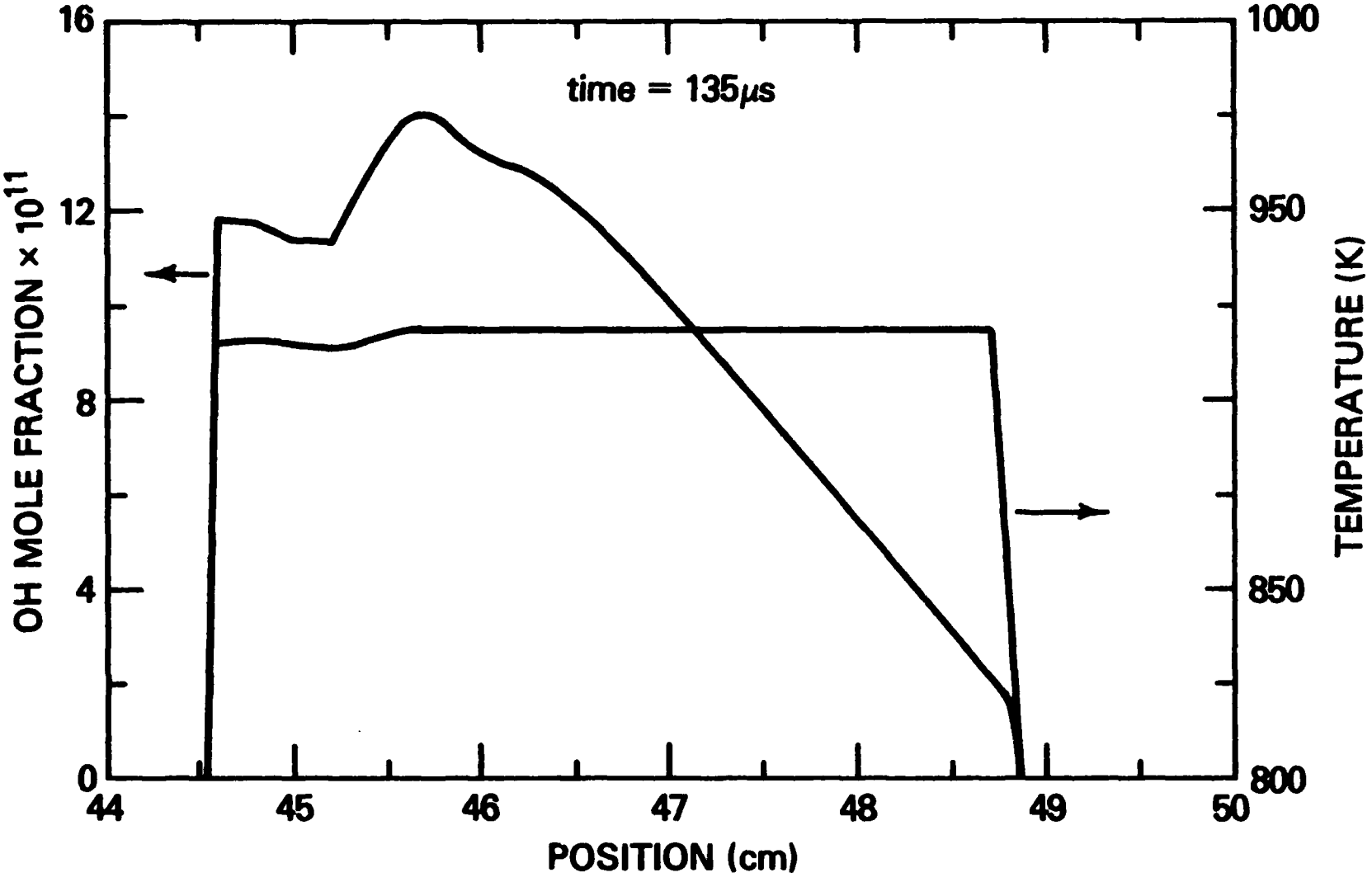

Figure 3. The spatial variation of the temperature and the OH mole fraction between the contact surface and the shock at 135 μs.

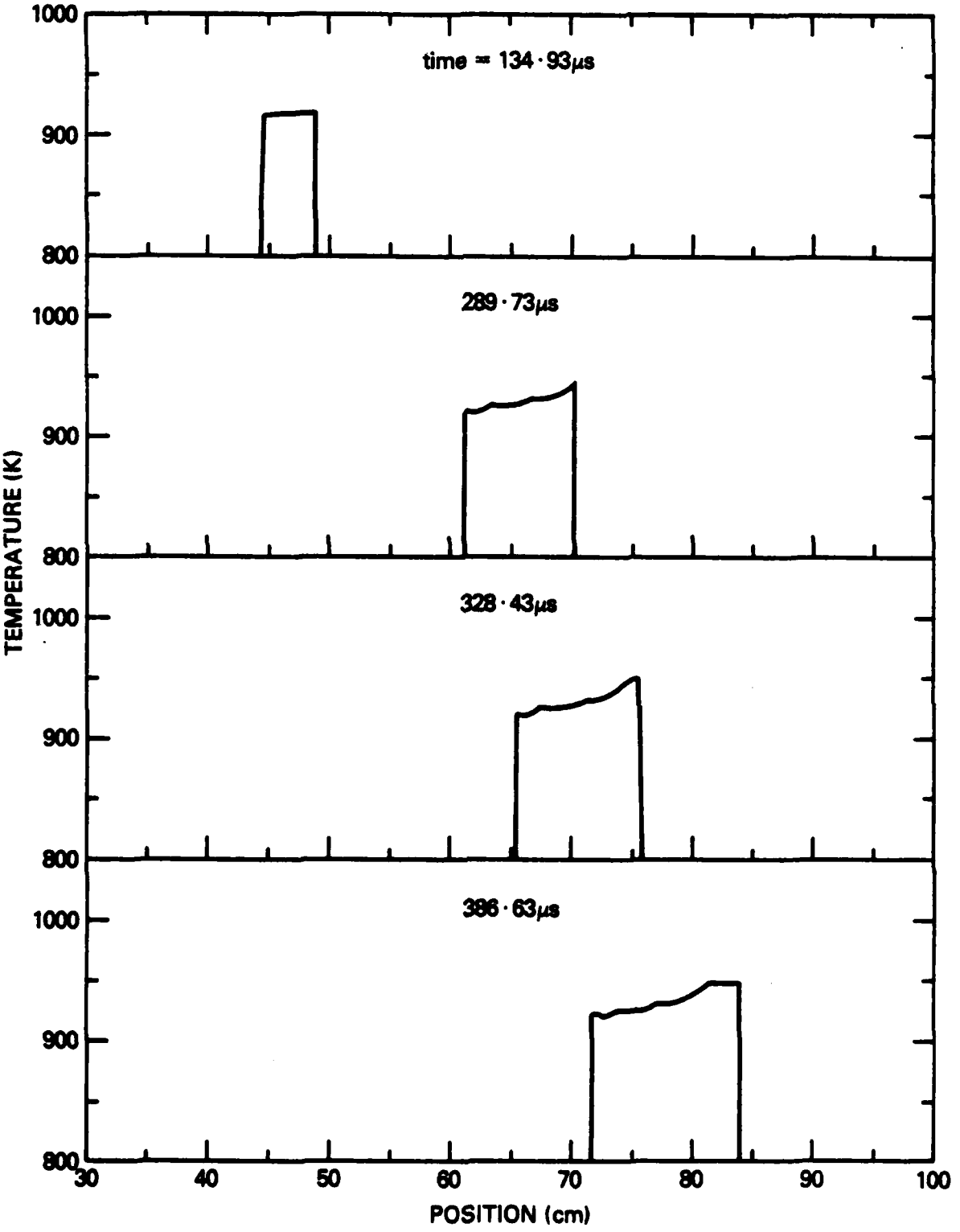

Figure 4. The spatial distribution of the temperature between the contact surface and the shock at four different times.

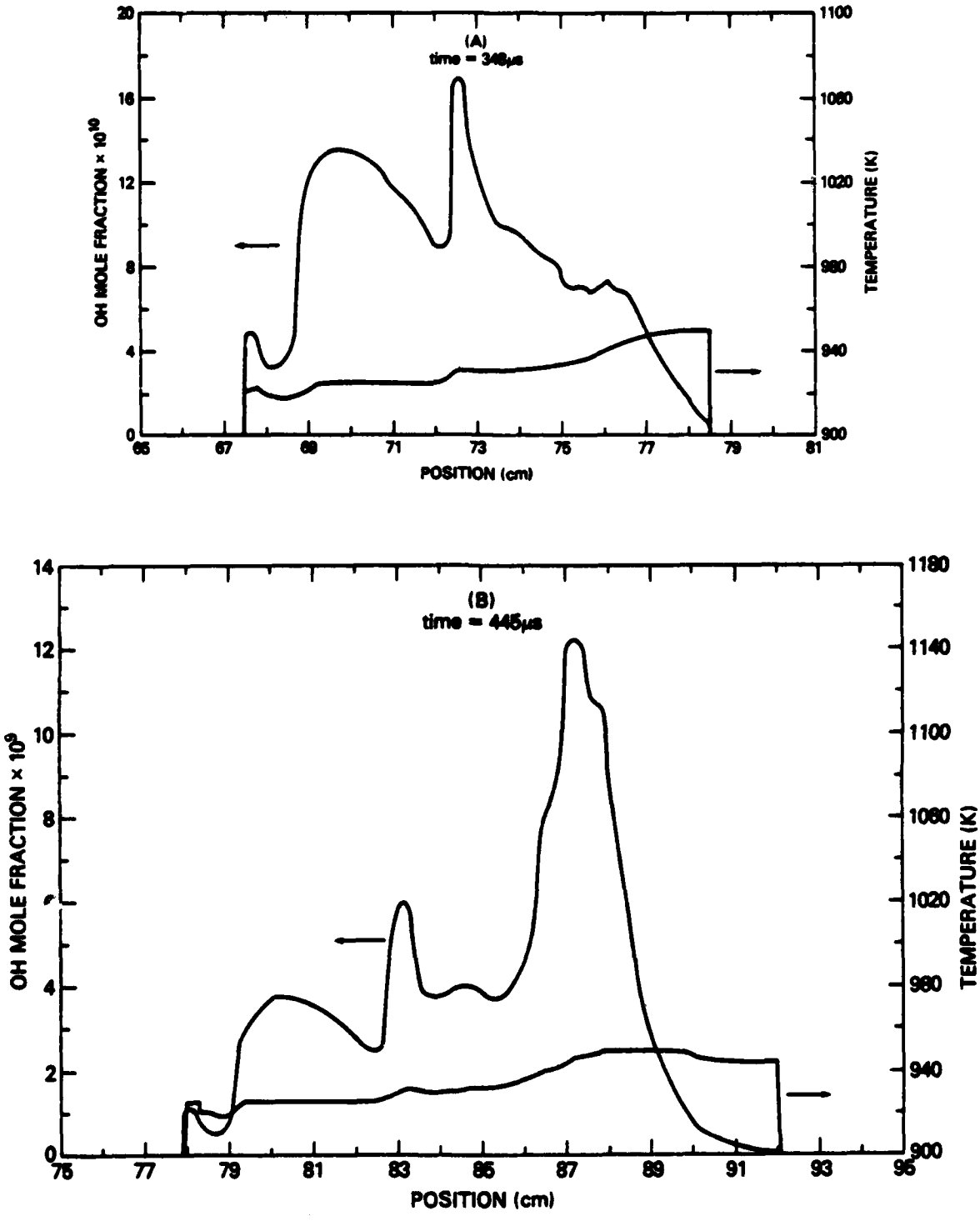

Figure 5. The spatial variation of the temperature and the OH mole fraction between the cntact surface and the shock at (a) 348 μs and (b) 445 μs.

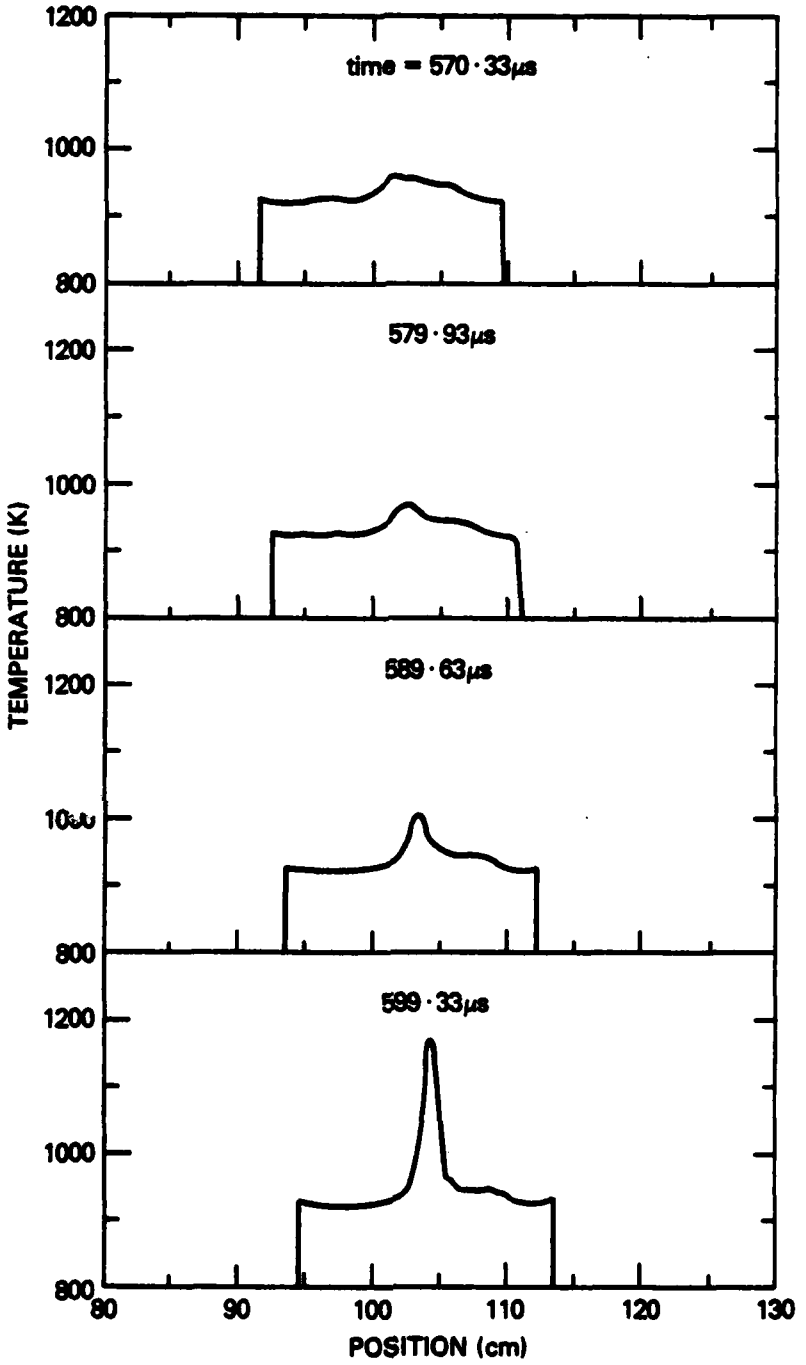

Figure 6. Time history of the development of a hot spot.

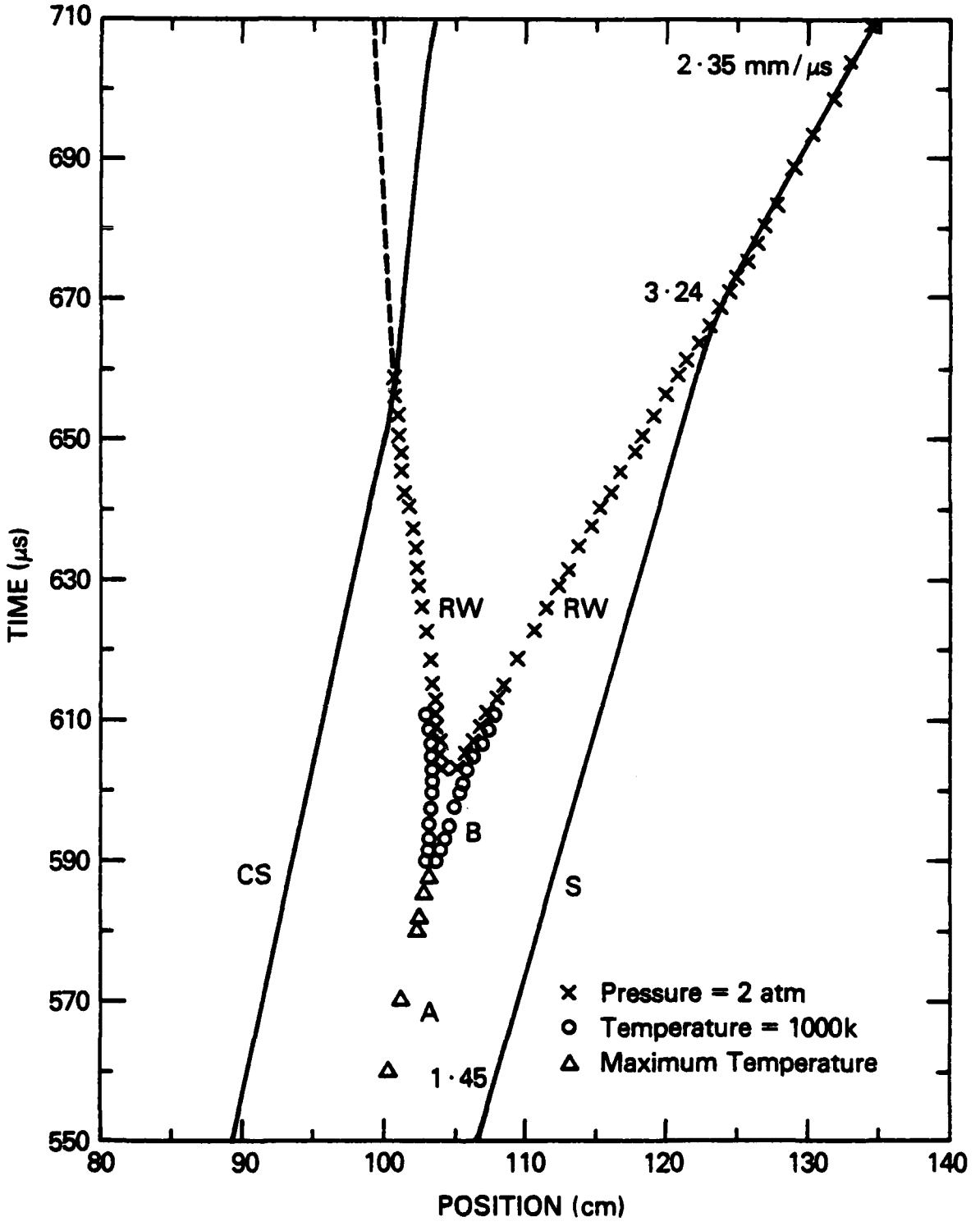

Figure 7. A position-time diagram showing the ignition of flamelets and the transition to detonation: A, hot spot and B, flamelets.

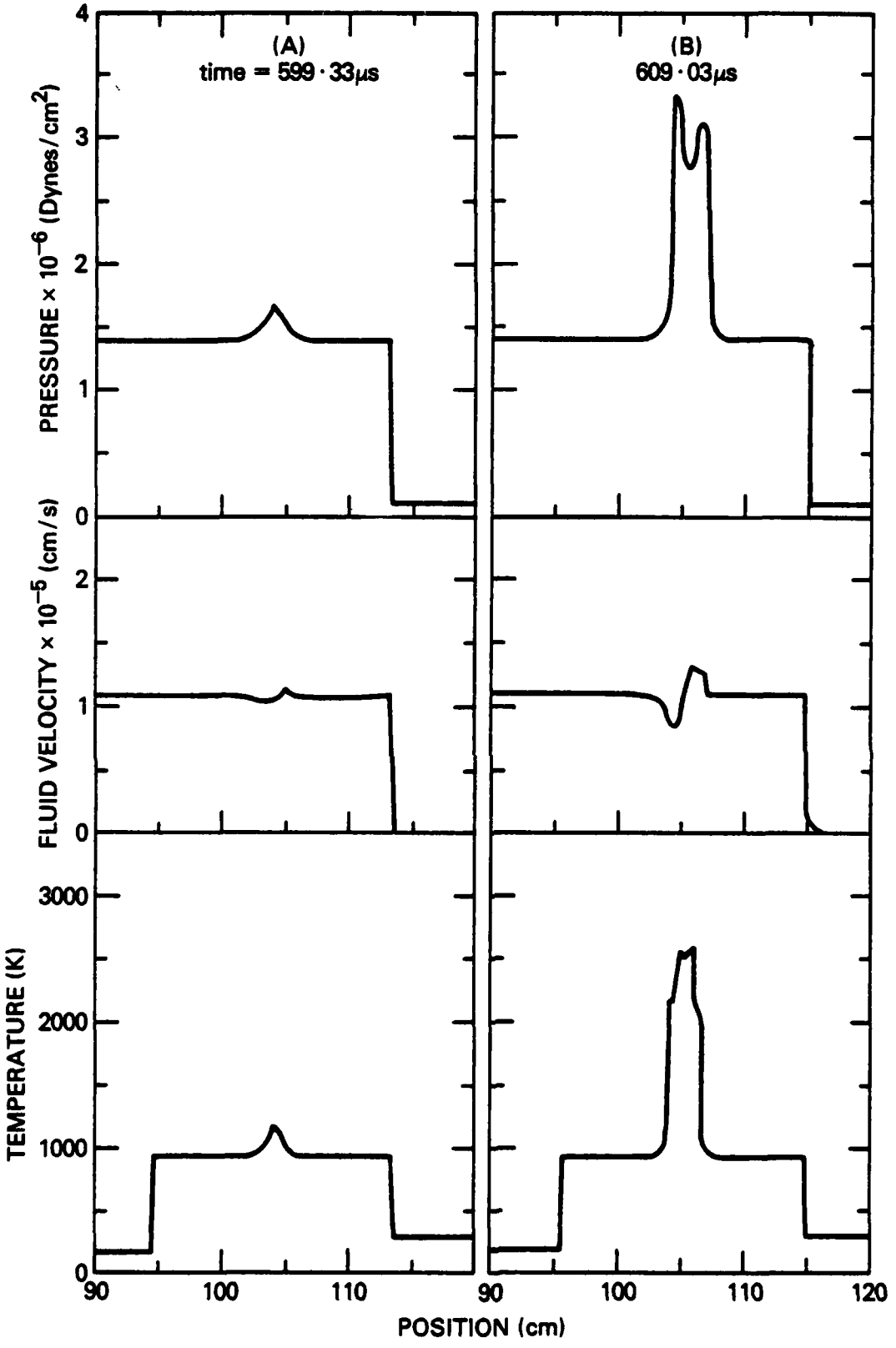

Figure 8. The pressure, velocity and temperature distributions across the system at (a) 599.33 μs and (b) 609.03 μs.

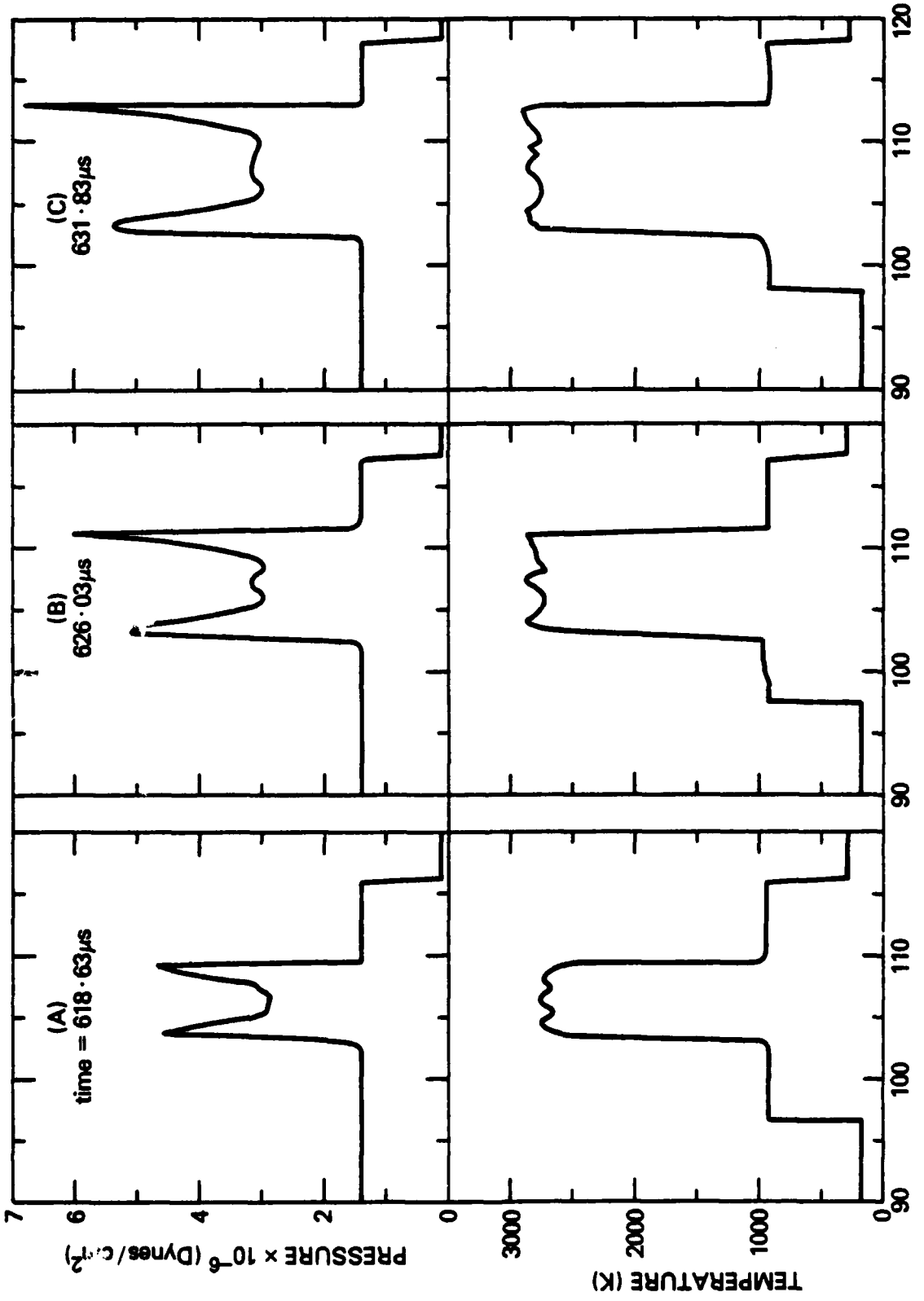

Figure 9. The pressure and temperature distributions across the system at (a) 618.63 μs, (b) 626.03 μs and (c) 631.83 μs.

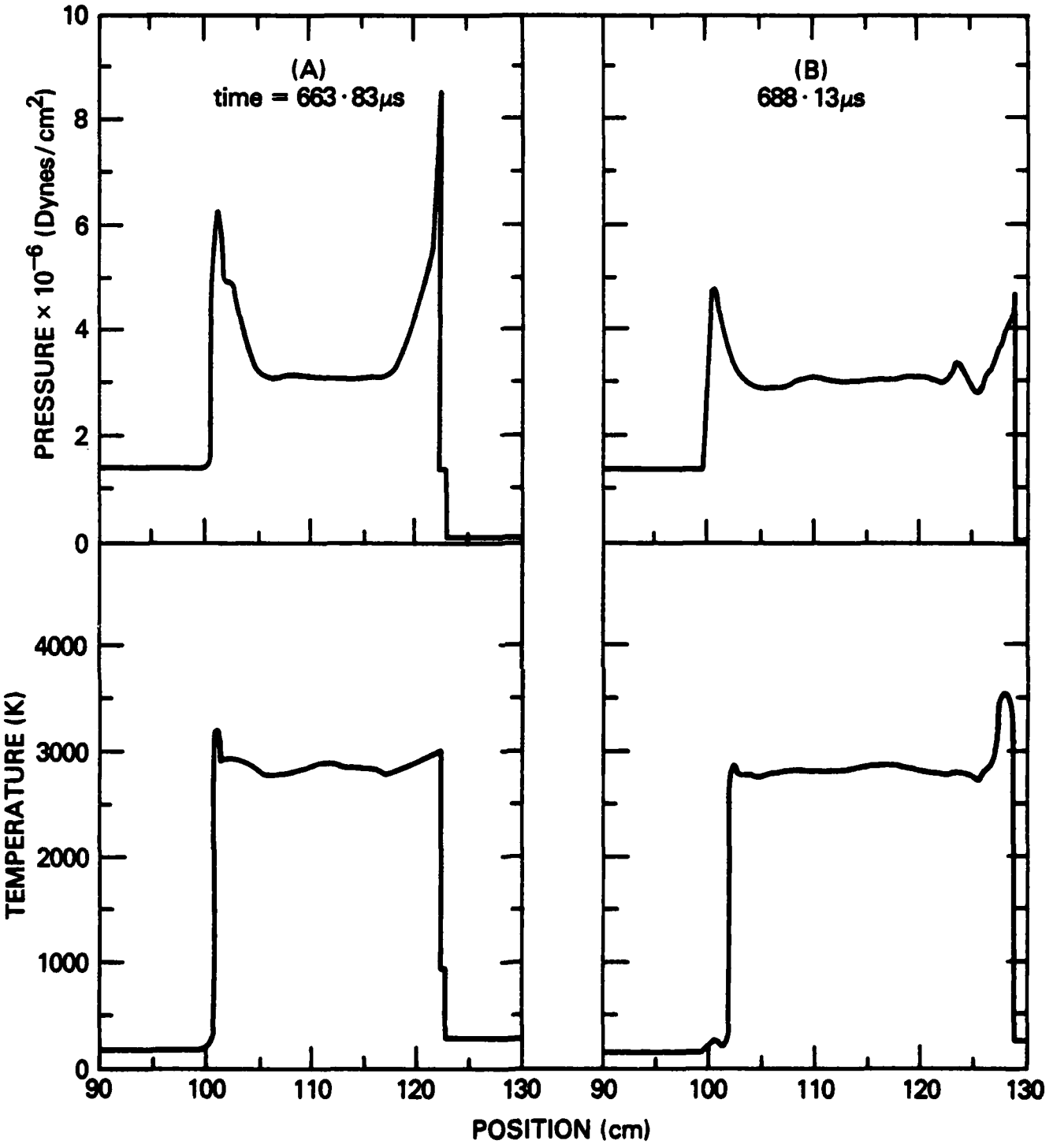

Figure 10. The pressure and temperature distributions across the system at (a) 663.83 μs and (b) 688.13 μs.

ACKNOWLEDGEMENTS

The authors greatfully acknowledge suggestions from and useful conversations with Jay Boris, Ted Young, and Antoni Oppenheim and editorial assistance from Mrs. Fran Rosenberg. This work has been supported by the Office of Naval Research through the Naval Research Laboratory.

REFERENCES

Bahn, G.S. (1968). Reaction Rate Compilation for H-O-N System, Gordon and Breach, New York.

Baulch, D.L., Drysdale, D.C., Horne, D.C., and Lloyd, A.C. (1972). Evaluated Kinetic data for High Temperature Reactions, Vol. 1, Butterworths, London.

Bazhenova, T.V., and Soloukhin, R.I. (1959). Gas Ignition Behind the Shock Wave. Seventh Symposium (International) on Combustion, The Combustion Institute, Pittsburgh, pp. 866-875.

Boris, J.P. (1976). Flux-Corrected Transport Modules for Solving Generalized Continuity Equations. Naval Research Laboratory Memorandum Report 3237, Washington, D.C.

Boris, J.P., and Book, D.L. (1976). Solution of Continuity Equations by the Method of Flux-Corrected Transport. In Methods of Computational Physics, Academic Press, New York, Vol. 16, Chap. 11, pp. 85-129.

Burks, T.L., and Oran, E.S. (1980). A Computational Study of the Chemical Kinetics of Hydrogen Combustion. Naval Research Laboratory Memorandum Report 4446, Washington, D.C.

Cohen, N., and Westberg, K.R. (1979). Data Sheets, The Aerospace Corporation, Los Angeles.

Edwards, D.H., Thomas, G.O., and Williams, T.L. (1981). Initiation of Detonation by Steady Planar Incident Shock waves, Combust. Flame. 43, 187.

Hampson, R.F., and Garvin, D. (1975). Chemical Kinetic and Photochemical Data for Modeling of Atmospheric Chemistry, NBS Technical Note 866, U.S. National Bureau of Standards, Washington, D.C.

Lee, J.H., and Ramamurthi, K. (1976). On the Concept of the Critical Size of a Detonation Kernal. Combust. Flame. 27, 331.

Lee, J.H. (1977). Initiation of Gaseous Detonation. Ann. Rev. Phys. Chem. 28, 75.

Lloyd, A.C. (1974). Evaluated and Estimated Kinetic Data for Gas Phase Reactions of the Hydroperoxyl Radical. Int. J. Chem. Kinetics. 6, 169.

Meyer, J.W., and Oppenheim, A.K. (1971a). On the Shock-Induced Ignition of Explosive Gases. Thirteenth Symposium (International) on Combustion, The Combustion Institute, Pittsburgh, pp. 1153-1164.

Meyer, J.W., and Oppenheim, A.K. (1971b). Coherence Theory of the Strong Ignition Limit. Combust. Flame. 17, 65.

Olson, D.B., and Gardiner, W.C. (1977). An Evaluation of Methane Combustion Mechanisms. J. Phys. Chem. 81, 2514.

Oran, E.S. Young, T.R., and Boris, J.P. (1979). Application of Time-Dependent Numerical Methods to the Description of Reactive Shocks. Seventeenth Symposium (International) on Combustion, The Combustion Institute, Pittsburgh, pp. 43-54.

Oran, E.S., and Boris, J.P. (1981a). Detailed Modelling of Combustion Systems. Prog. Energy Combust. Sci. 7, 1.

Oran, E.S., and Boris, J.P. (1981b). Weak and Strong Ignition-II. Naval Research Laboratory Memorandum Repot 4671, Washington, D.C. (also to appear in Combust. Flame).

Oran, E.S., Young, T.R., Boris, J.P., and Cohen, A. (1981a). Weak and Strong Ignition-I. Naval Research Laboratory Memorandum Report 4664, Washington, D.C. (also to appear in Combust. Flame)

Oran, E.S., Boris, J.P., Young, T., Flanigan, M., Burks, T., and Picone, M. (1981b). Numerical Simulations of Detonations in Hydrogen-Air and Methane-Air Mixtures. Eighteenth Symposium (International) on Combustion, The Combustion Institute, Pittsburgh, pp. 1641-1649.

Oran, E.S., Young, T.R. Boris, J.P., and Picone, J.M. (1982). A Study of Detonation Structure: The Formation of Unreacted Gas Pockets. Presented at the Nineteenth Symposium (International) on Combustion, The Combustion Institute, Pittsburgh.

Strehlow, R.A., Crooker, A.J., and Cusy, R.E. (1967). Detonation Initiation Behind an Accelerating Shock Wave. Combust. Flame. 11, 339.

Stull, D.R., and Prophet, H. (Eds.) (1971). JANAF Thermochemical Tables, Nat. Stand. Ref. Data Serv., No. 37, 2nd edition, U.S. National Bureau of Standards, Gaithersburg.

Urtiew, P.A., and Oppenheim, A.K. (1966). Experimental Observations of the Transition to Detonation in an Explosive Gas. Proc. Roy. Soc. A295, 13.

Urtiew, P.A., and Oppenheim, A.K. (1967). Detonative Ignition Induced by Shock Merging. Eleventh Symposium (International) on Combustion, The Combustion Institute, Pittsburgh, pp.665-670.

Williams, F.A. (1965). Combustion Theory, Addison-Wesley, Reading, p. 2.

Young, T.R., and Boris, J.P. (1977). A Numerical Technique for Solving Stiff Ordinary Differential Equations Associated with the Chemical Kinetics of Reactive-Flow Problems. J. Phys. Chem. 81, 2424.

Young, T.R. (1980). CHEMEQ - A Subroutine for Solving Stiff Ordinary Differential Equations. Naval Research Laboratory Memorandum Report 4091, Washington, D.C.